ACS APPLIED MATERIALS & INTERFACES

Research Article

www.acsami.org

Enhanced Photocatalytic Activity of ZnO Microspheres via Hybridization with $CuInSe_2$ and $CuInS_2$ Nanocrystals

Fengyu Shen,[†] Wenxiu Que,[†,*] Yucheng He,[†] Yuan Yuan,[†] Xingtian Yin,[†] and Gangfeng Wang[‡]

[†]Electronic Materials Research Laboratory, International Center for Dielectric Research, [‡]Department of Engineering Mechanics, SV Laboratory, Xi'an Jiaotong University, Xi'an 710049, Shaanxi, People's Republic of China

ABSTRACT: ZnO microspheres sensitized by $CuInSe_2$ and $CuInS_2$ nanoparticles, which were synthesized by a solvothermal method and have a size about 20 and 3.5 nm, respectively, were used to a photodegradation of rhodamine B under an irradiation of mercury lamp. Results show that the photocatalytic activities of the ZnO/$CuInSe_2$ and the ZnO/$CuInS_2$ are much higher than that of the ZnO microspheres because of a formation of the heterojunction in two systems. It is also noted that the ZnO/$CuInS_2$ exhibits a higher photocatalytic activity than the ZnO/$CuInSe_2$, which is probably related to more suitable band gap to sunlight for $CuInS_2$ nanocrystals and the larger specific surface due to a small size. Particularly, the ZnO/$CuInSe_2$/$CuInS_2$ shows the highest photocatalytic activities in all measured photocatalysts, which should be attributed to the formation of double heterojunctions among ZnO, $CuInSe_2$, and $CuInS_2$.

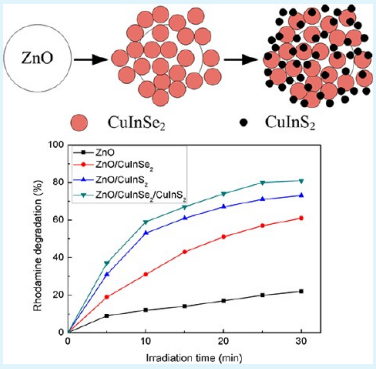

KEYWORDS: *ZnO, $CuInSe_2$, $CuInS_2$, Rhodamine B, heterojunction, photocatalytic activity*

1. INTRODUCTION

Organic pollution has been one of the most serious environmental problems during previous decades, and photocatalysis has been extensively used to eliminate toxic chemicals in the area of environmental remediation.[1−4] Semiconductor materials have attracted intensive interest in this area. Among various semiconductors, TiO_2 is known as the most efficient photocatalyst because of its high photosensitivity, chemical stability, and nontoxic nature.[5−7] In the past several years, ZnO, whose band gap is 3.37 eV, has been considered as a suitable alternative to TiO_2 because of its similar band gap energy and lower cost.[8−10] However, its large band gap along with a fast recombination rate of the photogenerated electron−hole pairs hinders its photocatalytic performance and limits its applications under the irradiation of sunlight.[11] Hence, to enhance the photocatalytic efficiency of ZnO, many improvements have been attempted. One of the most promising methods is to couple this wide band semiconductor with metals, such as Ag, Au, and Pt, or other semiconductors with different absorption band, such as TiO_2, SnO_2, CdS, ZnS and Bi_2O_3.[12−17] It has been reported that ZnO-based heterojunctions can inhibit the recombination of the photogenerated electron−hole pairs and enhance the photocatalytic activities.[18,19] In these cases, the energy levels of two kinds of semiconductor materials must match each other to form the staggered heterojunctions. For example, $CuInSe_2$ and $CuInS_2$ are two kinds of ideal sensitized materials to form heterojunction with those wide band gap semiconductors.

$CuInSe_2$ and $CuInS_2$ are I−III−VI_2 ternary compounds, with band-gaps of 1.04 and 1.53 eV, which match well to the solar spectrum,[20,21] and they have a large absorption coefficient and no highly toxic elements. Especially, optical absorption of the $CuInSe_2$ and $CuInS_2$ nanocrystals can be adjusted by varying their crystal size.[22−24] However, there have been only a few reports on photocatalytic activity of I−III−VI_2 ternary compounds. Zhang[25] reported the photocatalytic performance of ZnS-$CuInS_2$ nanocrystals, showing promising activity in the photodegradation of rhodamine B (RB). Zheng[26] used $CuInS_2$ as photocatalyst to catalyze hydrogen and a much high H_2 yield was obtained under the visible light irradiation. Recently, Zhou[27] reported that TiO_2 nanoparticles incorporated with $CuInS_2$ clusters can improve their photocatalytic activity for degradation of 4-nitrophenol. More recently, Tsuji[28] studied the activities of ZnS-$CuInS_2$−$AgInS_2$ solid solution photocatalysts on photolysis of water. But, above-mentioned these I−III−VI_2 ternary compounds were synthesized in situ, which is totally different from our research. Actually, our previous report indicated that the photocatalytic activity of TiO_2 sensitized by $CuInS_2$ nanocrystals shows a better performance than that of P25.[29]

Because of the promising properties of the $CuInSe_2$ and $CuInS_2$ nanocrystals sensitizing wide band gap semiconductors, herein we reported a new study on the ZnO/$CuInSe_2$ and the ZnO/$CuInS_2$ two-component nanoheterojunction systems and the ZnO/$CuInSe_2$/$CuInS_2$ three-component nanoheterojunction system. Three kinds of semiconductors were separately prepared. ZnO microspheres were synthesized by a hydrolysis of zinc salt in polyol medium, whereas the $CuInSe_2$ and $CuInS_2$ nanocrystals were prepared in noncoordinating solvents, which are oleylamine and octadecene, respectively. These different

Received: May 14, 2012
Accepted: July 9, 2012
Published: July 9, 2012

semiconductor materials were then mixed together by a low annealing temperature so as to form heterojunctions. Photocatalytic activities of the $ZnO/CuInSe_2$ and the $ZnO/CuInS_2$ heterojunctions and the $ZnO/CuInSe_2/CuInS_2$ double heterojunctions were investigated by evaluating the photocatalytic degradation of the RB aqueous solution at room temperature. Results indicate that the $CuInSe_2$ and $CuInS_2$ nanocrystals can enhance the photocatalytic activities of the ZnO microspheres and the sensitizing effect of the $CuInS_2$ nanocrystals is better than that of the $CuInSe_2$ nanocrystals.

2. EXPERIMENTAL SECTION

All chemicals used in this work were analytical-grade reagents and used without further purification. Deionized water with a resistance of 18.3MΩ·cm was used in the experiment.

2.1. Synthesis of the ZnO Microspheres. ZnO microspheres were synthesized by a hydrolysis of zinc salt at 180 °C, which is described in our previous report.[30] Typically, 0.01 mol $Zn(CH_3COO)_2{\cdot}2H_2O$ was added to 100 mL diethylene glycol with vigorous stirring and heated to 130 °C until the complete dissolution was achieved. Then, the solution was further heated to 180 °C and kept for 15 min. The obtained solution was centrifuged at the speed of 8000 rpm for 5 min and removed the supernatant. Subsequently, the precipitate was dispersed in ethanol and centrifuged at the speed of 8000 rpm for 10 min again and the ZnO microspheres were thus obtained.

2.2. Synthesis of the $CuInSe_2$ and $CuInS_2$ Nanocrystals. $CuInSe_2$ nanocrystals were synthesized in a noncoordinating oleylamine solvent.[31] Briefly, 2 mmol CuCl, 2 mmol $InCl_3{\cdot}4H_2O$, 4 mmol Se powder, and 10 mL oleylamine were loaded in a three-neck flask. The mixture solution was heated to 80 °C under a nitrogen atmosphere with a stirring for about 30 min to remove water and oxygen. The mixture solution was then quickly heated to 220 °C and incubated for 4 h. Subsequently, the reaction vessel was allowed to cool down to room temperature. Black $CuInSe_2$ nanocrystals were isolated by adding chloroform, precipitating with ethanol, and centrifuging at the speed of 10000 rpm for 5 min. The as-obtained sediment was then further redispersed in chloroform. The precipitation/centrifugation/dispersion cycle was repeated twice in order to eliminate byproducts and unreacted precursors. Thus, the $CuInSe_2$ nanocrystals were obtained by drying the suspension in oven at 80 °C. The $CuInS_2$ nanocrystals were synthesized in a noncoordinating octadecene solvent.[29] Briefly, 0.2 mmol CuCl and 0.2 mmol $InCl_3{\cdot}4H_2O$ were mixed with 2 mL of dodecanethiol and 8 mL of octadecene in a three-neck flask. The following procedures were the same as those of the synthesis of the $CuInSe_2$ nanocrystals.

2.3. Formation of Heterojunction Photocatalyst. The $CuInSe_2$ nanocrystals were first dispersed in chloroform and then mixed with the ZnO microspheres. Here, two kinds of materials were mixed through stirring until the solvent was completely volatilized. The $ZnO/CuInSe_2$ heterojunction photocatalyst was thus obtained by annealing the mixture at 300 °C for 15 min. For the preparation of the $ZnO/CuInS_2$ heterojunction photocatalyst, the above procedure was exactly followed with the exception of the $CuInS_2$ nanocrystals replacing of the $CuInSe_2$ nanocrystals. Finally, the $ZnO/CuInSe_2/CuInS_2$ double heterojunctions photocatalyst was obtained by hybridization of the $CuInS_2$ nanocrystals with the $ZnO/CuInSe_2$ heterojunction photocatalyst, followed byannealing at 300 °C for 15 min.

2.4. Characterization. X-ray diffraction (XRD) analysis was employed to characterize the crystallinity of the as-synthesized ZnO microspheres, the $CuInSe_2$ nanocrystals and the $CuInS_2$ nanocrystals, which employs a D/max 2400 X Series X-ray diffractometer. The X-ray radiation source is Cu Kα, obtained at 40 kV, 100 mA, and the scanning speed was 10° min^{-1} at a step of 0.02°. A transmission electron microscopy (TEM, JEM2100, JEOL Inc., Japan) was employed to observe the morphological properties of the $CuInSe_2$, $CuInS_2$ and heterojunction photocatalysts. A field emission scanning electron microscopy (FESEM, JSM-7000F, JEOL Inc. Japan) was employed to characterize the morphology of the ZnO microspheres. UV−vis absorption spectra of the samples were obtained by a JASCO V-570 UV/vis/NIR spectrometer.

2.5. Photocatalytic Activity Measurement. Photocatalytic activities of the photocatalyst samples were evaluated by observe the degradation of the RB aqueous solution at ambient temperature using a 300 W high-pressure mercury lamp as light source. Typically, 0.03 g of the photocatalyst was added to 100 mL of 10 mg/L RB aqueous solution in a quartz glass container. The solution was continuously stirred in the dark for 2 h to ensure the establishment of an adsorption−desorption equilibrium between the photocatalyst and the RB before irradiation. A certain volume of the suspension solution was withdrawn at a sequence of time intervals. After disposal of the photocatalyst by a centrifugation, the concentration of residual RB aqueous solution was measured by the UV−vis spectrophotometer at 554 nm to calculate the degradation of the RB based on the Beer−Lambert Law.[32] The degradation efficiency of the RB can be defined as follows

$$\text{degradation}\ (\%) = \frac{A_0 - A_t}{A_0} \times 100\% \quad (1)$$

where A_0 is the initial concentration of the RB and A_t is the concentration of the RB at reaction time t (min). It was assumed that the photocatalytic degradation of the RB follows a pseudo-first-order kinetic[33,34] and the kinetic reaction can be expressed as follows

$$A_t = A_0 e^{-kt} \quad (2)$$

where k (min^{-1}) is the degradation rate constant.

3. RESULTS AND DISCUSSION

Figure 1 (a) shows the XRD pattern of the ZnO microspheres. All of the diffraction peaks can be indexed to the hexagonal phase of ZnO (JPCDS, NO. 36−1451). It can be seen that these diffraction peaks are sharp and intense, indicating its highly crystalline nature. Figure 1b shows the FESEM image of the ZnO microspheres. It reveals that the as-prepared ZnO

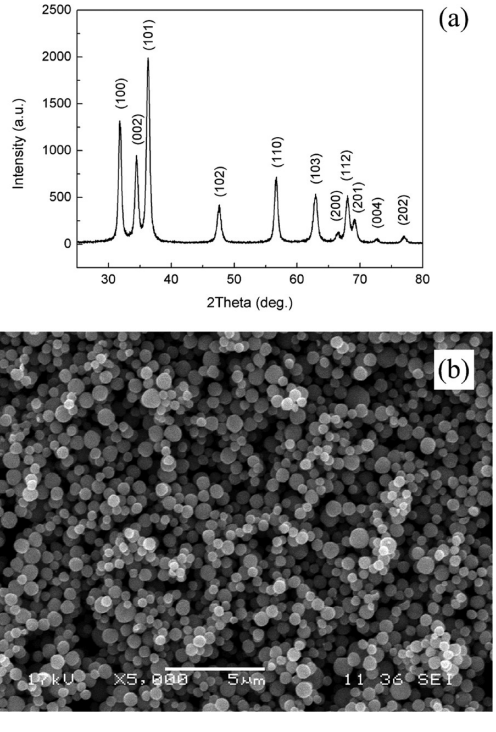

Figure 1. ZnO microspheres: (a) XRD pattern and (b) FESEM image.

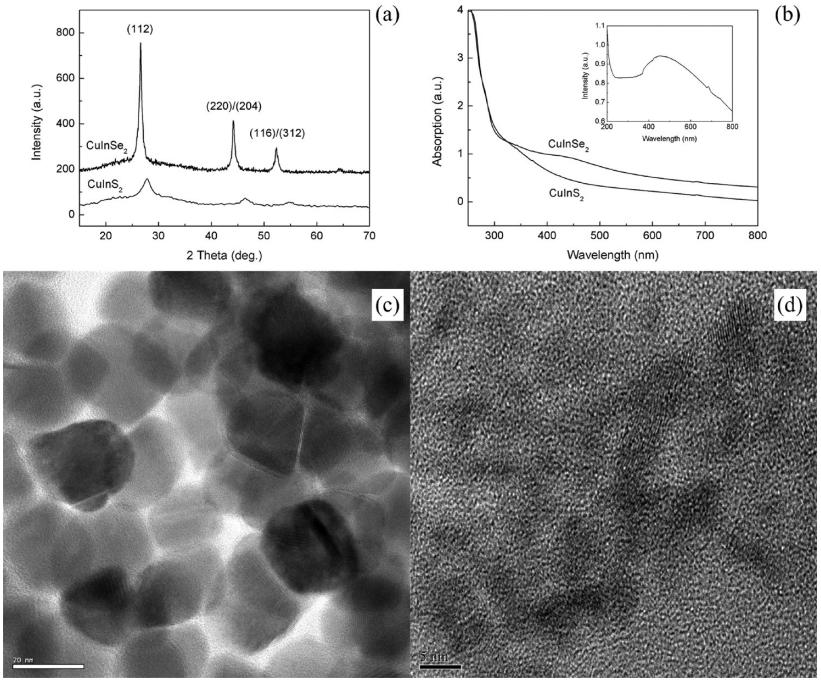

Figure 2. (a) XRD patterns; (b) UV−vis absorption spectra of $CuInSe_2$ and $CuInS_2$ nanocrystals, the inset shows the UV−vis absorption spectrum of $ZnO/CuInSe_2/CuInS_2$ heterojunction photocatalyst; (c) TEM image of $CuInSe_2$ nanocrystals; (d) TEM image of $CuInS_2$ nanocrystals.

microspheres are dispersive and uniform, and its size is about 500 nm.

Figure 2 shows the XRD patterns, UV−vis absorption spectra, and TEM images of the as-synthesized $CuInSe_2$ and $CuInS_2$ nanocrystals. XRD patterns as shown in Figure 2 (a) reveal that they have a similar crystal structure. In fact, both of $CuInSe_2$ and $CuInS_2$ are chalcopyrite compounds. According to the Debye−Scherrer formula, it can be obtained that the size of $CuInSe_2$ is larger than that of $CuInS_2$. UV−vis absorption spectrum reflects the photoresponse of the materials. It can be seen from Figure 2b that the absorption of $CuInSe_2$ nanocrystals and $CuInS_2$ nanocrystals almost covers the entire visible region and the UV region. The TEM images of the $CuInSe_2$ and $CuInS_2$ nanocrystals as shown in images c and d in Figure 2 indicate that two kinds of nanoparticles are dispersive and their sizes are about 20 and 3.5 nm, respectively.

The photocatalytic degradation kinetics of the RB aqueous solution, which has an addition of the pure ZnO microspheres, the $ZnO/CuInSe_2$ and the $ZnO/CuInS_2$, respectively, is shown in Figure 3. Here, a mass ratio of ZnO and $CuInSe_2$ as well as that of ZnO and $CuInS_2$ is 14:1. Results reveal that 22, 45, and 82% of the RB aqueous solution can be photodegraded under 30 min irradiation by the ZnO microspheres, the $ZnO/CuInSe_2$,and the $ZnO/CuInS_2$ photocatalysts, respectively, indicating that an introduction of the $CuInSe_2$ or $CuInS_2$ nanocrystals can improve the photocatalytic performance of the ZnO microspheres due to a formation of the $ZnO/CuInSe_2$ or $ZnO/CuInS_2$ heterojunction. Especially, the photocatalytic activity of the $ZnO/CuInS_2$ heterojunction photocatalyst is better than that of the $ZnO/CuInSe_2$ heterojunction photocatalyst, which is probably related to the following two aspects.

(1) Because the optimal band gap for sunlight is about 1.45 eV, the $CuInS_2$ nanocrystals matches better with sunlight than the $CuInSe_2$ nanocrystal. Thus, the absorption efficiency of the $CuInS_2$ nanocrystals to sunlight is higher than that of the $CuInSe_2$ nanocrystal.

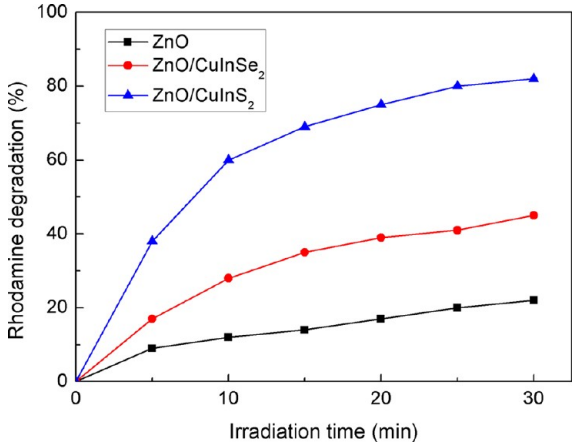

Figure 3. Photocatalytic degradation kinetics of RB aqueous solution with an addition of ZnO microspheres, $ZnO/CuInSe_2$ (with mass ratio of 14:1) heterojunction photocatalyst, and $ZnO/CuInSe_2$ (with mass ratio of 14:1) heterojunction photocatalyst.

(2) The size of the $CuInS_2$ nanocrystals is smaller than that of the $CuInSe_2$ nanocrystals, which could bring quantum effect. Moreover, smaller size means larger specific surface.

Quantum effect takes place at particle dimensions smaller than the Wannier-Mott exciton Bohr radius of the corresponding macroscopic bulk phase. Wannier−-Mott exciton Bohr radius, R_B, can be calculated according to following formula[35]

$$R_B = \varepsilon_\infty \left(\frac{1}{m^*_e} + \frac{1}{m^*_h} \right) a_B \quad (3)$$

where ε_∞ is the dielectric constant of the bulk material, and m^*_e and m^*_h are the reduced masses of the electron and hole, respectively. Taking the $CuInSe_2$ bulk values of $\varepsilon_\infty = 14.7$, $m^*_e = 0.08$, $m^*_h = 0.71$, and the $CuInS_2$ bulk values of $\varepsilon_\infty = 11$, m^*_e

dx.doi.org/10.1021/am3008533 | ACS Appl. Mater. Interfaces 2012, 4, 4087−4092

=0.16, m^*_h = 1.3,[36−38] we calculate the Wannier-Mott exciton Bohr radii of the $CuInSe_2$ and $CuInS_2$ bulk are 10.6 and 4.1 nm, respectively. In our experiment, the particle size of the $CuInSe_2$ nanocrystals (~20 nm) is larger than its corresponding Wannier-Mott exciton Bohr radius, whereas the particle size of the $CuInS_2$ nanocrystals (~3.5 nm) is smaller than its corresponding Wannier−Mott exciton Bohr radius.

In order to further explore the sensitizing effect of the $CuInSe_2$ and $CuInS_2$ nanocrystals, the photocatalytic activities of the ZnO microspheres and the sensitizers with a different mass ratio of 5:1 are also investigated and results are shown in Figure 4, indicating that 61 and 73% of the RB aqueous

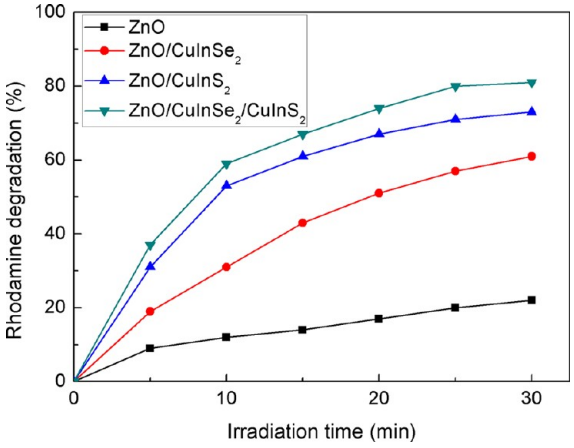

Figure 4. Photocatalytic degradation kinetics of RB aqueous solution with an addition of ZnO microspheres, $ZnO/CuInSe_2$ (with mass ratio of 5:1) heterojunction photocatalyst, $ZnO/CuInSe_2$ (with mass ratio of 5:1) heterojunction photocatalyst, and $ZnO/CuInSe_2/CuInS_2$ (with mass ratio of 10:1:1) double heterojunctions photocatalyst.

solution can be photodegraded under 30 min irradiation by the $ZnO/CuInSe_2$ and $ZnO/CuInS_2$ photocatalysts, respectively. Obviously, the photocatalytic performance of the $ZnO/CuInS_2$ heterojunction photocatalyst is still better than that of the $ZnO/CuInSe_2$ heterojunction photocatalyst. Additionally, as compared with the results as shown in Figure 3, it is easy to find that the photocatalytic performance of the $ZnO/CuInSe_2$ increases a little, whereas the photocatalytic performance of the $ZnO/CuInS_2$ decreases a little with increasing the content of the sensitizer. Interestingly, when 50% of the $CuInSe_2$ nanocrystals and 50% of the $CuInS_2$ nanocrystal replace of the $CuInS_2$ nanocrystals to sensitize the ZnO microspheres, the photocatalytic activity of the as-obtained $ZnO/CuInSe_2/CuInS_2$ photocatalyst is better than that of the $ZnO/CuInS_2$ heterojunction photocatalyst. It can be seen from Figure 4 that about 81% of the RB can be photodegraded by the $ZnO/CuInSe_2/CuInS_2$ photocatalyst under 30 min irradiation. Here, the mass ratio of ZnO, $CuInSe_2$, and $CuInS_2$ in the $ZnO/CuInSe_2/CuInS_2$ system is 10:1:1. To further investigate the photocatalytic activities of the ZnO and the $ZnO/CuInSe_2/CuInS_2$, an UV filter is used to filter out UV and the results are shown in Figure 5. It can be seen that the photocatalytic activity of the $ZnO/CuInSe_2/CuInS_2$ is still higher than that of the ZnO, but the photocatalytic activities of the ZnO and the $ZnO/CuInSe_2/CuInS_2$ are worse than those of the samples under the irradiation of mercury lamp without an UV filter. In 30 min, 14 and 64% of the RB can be photodegraded by the ZnO and the $ZnO/CuInSe_2/CuInS_2$ photocatalysts, respectively.

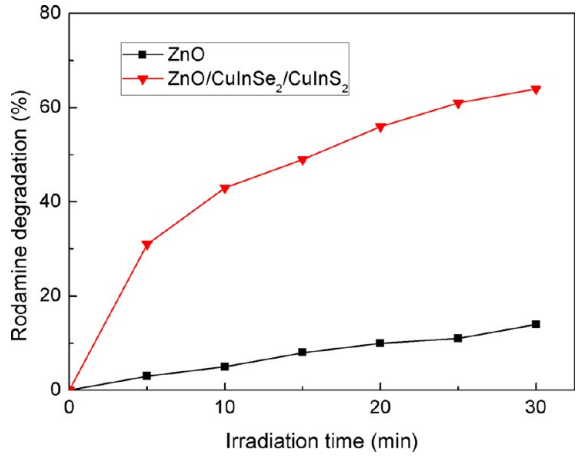

Figure 5. Photocatalytic degradation kinetics of RB aqueous solution with an addition of ZnO microspheres, $ZnO/CuInSe_2/CuInS_2$ (with mass ratio of 10:1:1) double heterojunctions photocatalyst under an irradiation of mercury lamp with an UV filter.

The degradation rate k of all the evaluated photocatalysts is presented in Table 1. These results indicate that the

Table 1. Values of the Degradation Rate Constant k for different photocatalysts

photocatalyst	k (min^{-1}) (average)
ZnO	0.008
$ZnO/CuInSe_2$-14:1	0.020
$ZnO/CuInS_2$-14:1	0.057
$ZnO/CuInSe_2$-5:1	0.031
$ZnO/CuInS_2$-5:1	0.044
$ZnO/CuInSe_2/CuInS_2$-10:1:1	0.055
ZnO (with UV filter)	0.005
$ZnO/CuInSe_2/CuInS_2$-10:1:1 (with UV filter)	0.034

photocatalytic performance of the hybridization photocatalysts is obviously improved as compared to that of the pure ZnO microspheres. The preparation procedure of the $ZnO/CuInSe_2/CuInS_2$ double heterojunctions system is shown in Figure 6. First, 8.3 wt % of the $CuInSe_2$ nanocrystals are

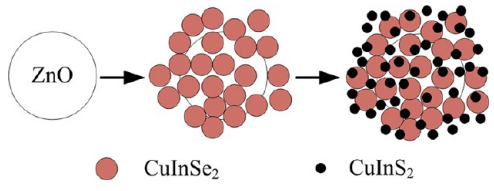

Figure 6. Formation scheme for the $ZnO/CuInSe_2/CuInS_2$ double heterojunctions system.

blended with the ZnO microspheres, followed a heat treatment at 300 °C for 30 min to form the $ZnO/CuInSe_2$ heterojunction. Then, 8.3 wt % of $CuInS_2$ nanocrystals are blended with the $ZnO/CuInSe_2$ heterojunction, followed a heat treatment at 300 °C for 30 min again to form the $ZnO/CuInSe_2/CuInS_2$ double heterojunctions.

To visualize the hybridization between the ZnO microsphere and the $CuInSe_2$ nanocrystals as well as the $CuInS_2$ nanocrystals in the $ZnO/CuInS_2$ system and the $ZnO/CuInSe_2/CuInS_2$ system, the $ZnO/CuInS_2$ sample and the $ZnO/CuInSe_2/CuInS$ sample as presented in Figure 4 were

characterized by TEM. Figure 7 (a) shows a representative high-resolution TEM (HRTEM) image of the ZnO/$CuInS_2$ sample. The visible lattice fringe of the $CuInS_2$ nanocrystals indicates that they are adhered to the ZnO microspheres. The particle size of the ZnO microspheres is too large as compared to the $CuInS_2$ nanocrystals, which prevents the simultaneous display of the lattice of ZnO and $CuInS_2$. Figure 7b presents a representative TEM image of the ZnO/$CuInSe_2$/$CuInS_2$ double heterojunctions photocatalyst. The lattice of $CuInSe_2$ and $CuInS_2$ can be clearly distinguished and some $CuInS_2$ nanocrystals are adhered to the $CuInSe_2$ nanocrystals and the others are adhered to the ZnO microspheres, which results in better photocatalytic activity.

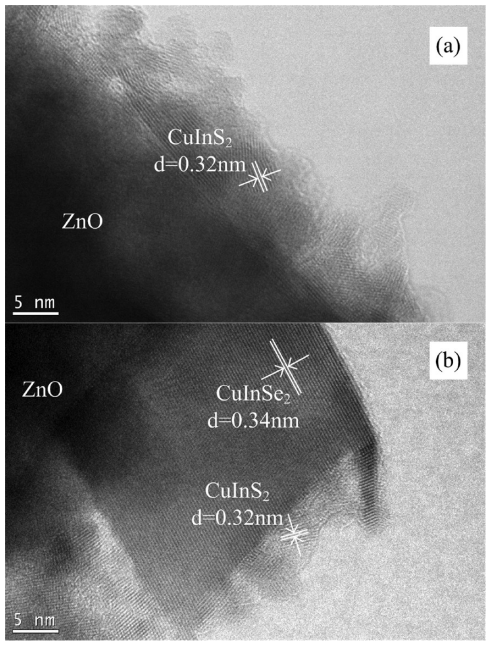

Figure 7. HRTEM images of the interface between (a) ZnO and $CuInS_2$ (with mass ratio of 5:1) and (b) ZnO, $CuInSe_2$, and $CuInS_2$ (with mass ratio of 10:1:1).

On the basis of the above results, the photocatalytic performance of the ZnO microspheres can be greatly enhanced by introducing $CuInSe_2$ and $CuInS_2$ nanocrystals. The inset in Figure 2b shows the absorption spectrum of the ZnO/$CuInSe_2$/$CuInS_2$ double heterojunctions photocatalyst. There is a great absorption in 400−600 nm region. The enhanced photocatalytic activity is ascribed to not only that the $CuInSe_2$ and $CuInS_2$ nanocrystals can improve the absorption efficiency of the photocatalysts to solar energy but also that the formation of the heterojunction that can inhibit the recombination of the photogenerated electron−hole pairs. Actually, the relative position of energy level of the hybridization semiconductors affects the transfer of electrons and holes and finally affects photocatalytic performance. Figure 8 (a) illustrates the relative energy levels of ZnO, $CuInSe_2$ and $CuInS_2$ before contact. ZnO is an n-type semiconductor whose Fermi energy level is located to the conduction band, while $CuInSe_2$ and $CuInS_2$ are p-type semiconductors whose Fermi energy levels lie close to valence band.[39] When ZnO is in contact with $CuInSe_2$ to form a heterojunction, their Fermi energy levels reach equilibration. Meanwhile, the energy bands of ZnO shift downward along with the Fermi energy level, whereas the energy bands of $CuInSe_2$ shift upward along with the Fermi energy level. Then, the photogenerated electrons transfer from the conduction band of $CuInSe_2$ to the conduction band of ZnO, whereas the photogenerated holes transfer in the opposite direction along with valence bands. The whole process is illustrated in Figure 8b. A similar situation also happens in the ZnO/$CuInS_2$ heterojunction system, which is shown in Figure 8c. Figure 8d illustrates the separation and transmission of the photo-

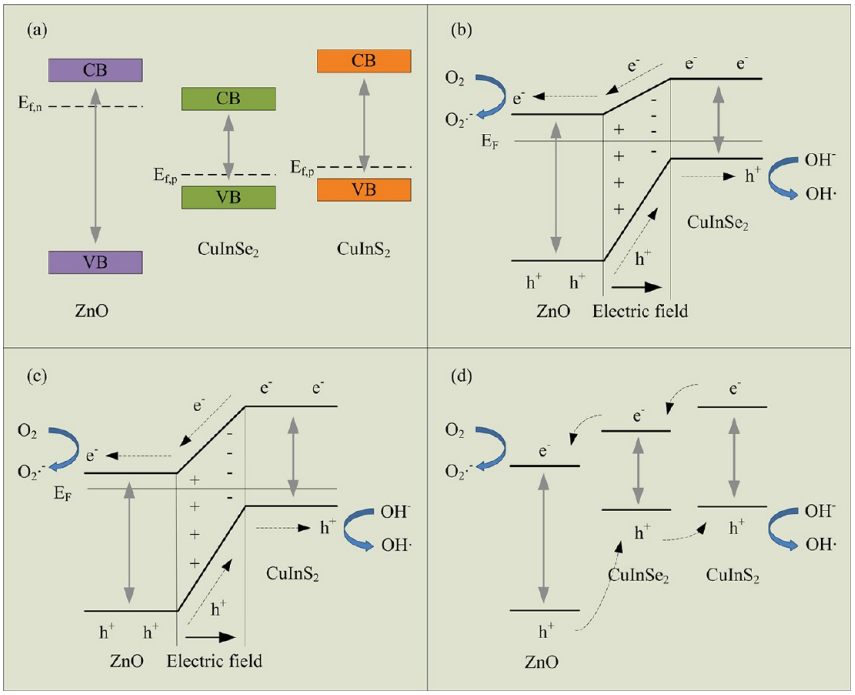

Figure 8. Diagram of the (a) band energy of ZnO, $CuInSe_2$ and $CuInS_2$ before contact, and the electron−hole pair separation and transmission in (b) ZnO/$CuInSe_2$ heterojunction system, (c) ZnO/$CuInS_2$ heterojunction system, and (d) ZnO/$CuInSe_2$/$CuInS_2$ double heterojunction system.

dx.doi.org/10.1021/am3008533 | ACS Appl. Mater. Interfaces 2012, 4, 4087−4092

generated electron−hole pairs in the ZnO/$CuInSe_2$/$CuInS_2$ double heterojunctions system. When the Fermi energy levels reach equilibration, the photogenerated electrons transfer from the conduction band of $CuInS_2$ to that of $CuInSe_2$ and then to that of ZnO, whereas the photogenerated holes transfer in the opposite direction along with valence bands. The hybridization of the ZnO microspheres with the $CuInSe_2$ and $CuInS_2$ nanocrystals inhibits the recombination of the electron−hole pairs, thus resulting in more holes can participate in the photooxidation process.

4. CONCLUSIONS

The $CuInSe_2$ and $CuInS_2$ nanocrystals have been successfully synthesized by the solvothermal method and used to couple with the ZnO microspheres prepared by the hydrolysis method to form the ZnO/$CuInSe_2$ or ZnO/$CuInS_2$ heterojunction, which is beneficial for the photodegradation of the RB. Results indicate that the photocatalytic efficiency of the ZnO/$CuInSe_2$ and ZnO/$CuInS_2$ heterojunction photocatalysts is always higher than that of the pure ZnO microspheres photocatalyst, and the photocatalytic performance of the ZnO/$CuInS_2$ heterojunction photocatalyst is better than that of the ZnO/$CuInSe_2$ heterojunction photocatalyst. However, the double heterojunctions photocatalyst of the ZnO/$CuInSe_2$/$CuInS_2$ shows the highest photocatalytic activities in all evaluated heterojunction photocatalysts. The enhanced photocatalytic activity is mainly ascribed to the formation of the heterojunctions, which can improve the absorption efficiency to light and inhibit the recombination of the photogenerated electron−hole pairs.

AUTHOR INFORMATION

Corresponding Author

*Tel.: +86-29-82668679. Fax: +86-29-82668794. E-mail: wxque@mail.xjtu.edu.cn.

Notes

The authors declare no competing financial interest.

ACKNOWLEDGMENTS

This work was supported by the Major Program of the National Natural Science Foundation of China (no. 90923012) and the Fundamental Research Funds for the Central Universities.

REFERENCES

(1) Asahi, R.; Morikawa, T.; Ohwaki, T.; Aoki, K.; Taga, Y. *Science* **2001**, *293*, 269−271.
(2) Hoffmann, M. R.; Martin, S. T.; Choi, W. Y.; Bahnemann, D. W. *Chem. Rev.* **1995**, *95*, 69−96.
(3) Tang, Y. X.; Wee, P. X.; Lai, Y. K.; Wang, X. P.; Gong, D. G.; Kanhere, P. D.; Lim, T. T.; Dong, Z. L.; Chen, Z. *J. Phys. Chem. C* **2012**, *116*, 2772−2780.
(4) Yin, L. F.; Shen, Z. Y.; Niu, J. F.; Chen, J.; Duan, Y. P. *Environ. Sci. Technol.* **2010**, *44*, 9117−9122.
(5) Pang, Y. L.; Abdullah, A. Z.; Bhatia, S. *Appl. Catal. B* **2010**, *100*, 393−402.
(6) Han, F.; Kambala, V. S. R.; Srinivasan, M.; Rajarathnam, D.; Naidu, R. *Appl. Catal. A* **2009**, *359*, 25−40.
(7) Inoue, T.; Fujishima, A.; Konishi, S.; Honda, K. *Nature* **1979**, *277*, 637−638.
(8) Kuo, C. L.; Kuo, T. J.; Huang, M. H. *J. Phys. Chem. B* **2005**, *109*, 20115−20121.
(9) Wan, Q.; Wang, T. H.; Zhao, J. C. *Appl. Phys. Lett.* **2005**, 87.
(10) Wang, Z.; Song, J. *Science* **2006**, *312*, 242−246246.
(11) Burda, C.; Lou, Y. B.; Chen, X. B.; Samia, A. C. S.; Stout, J.; Gole, J. L. *Nano Lett.* **2003**, *3*, 1049−1051.
(12) Wu, J. J.; Tseng, C. H. *Appl. Catal. B-Environ.* **2006**, *66*, 51−57.
(13) Pawinrat, P.; Mekasuwandumrong, O.; Panpranot, J. *Catal. Commun.* **2009**, *10*, 1380−1385.
(14) Li, P.; Wei, Z.; Wu, T.; Peng, Q.; Li, Y. D. *J. Am. Chem. Soc.* **2011**, *133*, 5660−5663.
(15) Li, C. Z.; Zhang, J. Y.; Yang, J. A.; Wang, T. M.; Lv, X.; Tang, Z. L. *Appl. Catal. A-Gen.* **2011**, *402*, 80−86.
(16) Zhang, Z.; Shao, C.; Li, X.; Wang, C.; Zhang, M.; Liu, Y. *ACS Appl. Mater. Interfaces* **2010**, *2*, 2915−2923.
(17) Xu, C.; Cao, L. X.; Su, G.; Liu, W.; Liu, H.; Yu, Y. Q.; Qu, X. F. *J. Hazard. Mater.* **2010**, *176*, 807−813.
(18) Hameed, A.; Gombac, V.; Montini, T.; Graziani, M.; Fornasiero, P. *Chem. Phys. Lett.* **2009**, *472*, 212−216.
(19) Wang, X. W.; Liu, G.; Chen, Z. G.; Li, F.; Wang, L. Z.; Lu, G. Q.; Cheng, H. M. *Chem. Commun.* **2009**, 3452−3454.
(20) Xu, J.; Lee, C. S.; Tang, Y. B.; Chen, X.; Chen, Z. H.; Zhang, W. J.; Lee, S. T.; Zhang, W. X.; Yang, Z. H. *ACS Nano* **2010**, *4*, 1845−1850.
(21) Yue, W.; Han, S.; Peng, R.; Shen, W.; Geng, H.; Wu, F.; Tao, S.; Wang, M. *J. Mater. Chem.* **2010**, *20*, 7570−7578.
(22) Wang, X. L.; Pan, D. C.; Weng, D.; Low, C. Y.; Rice, L.; Han, J. Y.; Lu, Y. F. *J. Phys. Chem. C* **2010**, *114*, 17293−17297.
(23) Omata, T.; Nose, K.; Otsuka-Yao-Matsuo, S. *J. Appl. Phys.* **2009**, *105*073106.
(24) Chiang, M. Y.; Chang, S. H.; Chen, C. Y.; Yuan, F. W.; Tuan, H. Y. *J. Phys. Chem. C* **2011**, *115*, 1592−1599.
(25) Zhang, W. J.; Zhong, X. H. *Inorg. Chem.* **2011**, *50*, 4065−4072.
(26) Zheng, L.; Xu, Y.; Song, Y.; Wu, C. Z.; Zhang, M.; Xie, Y. *Inorg. Chem.* **2009**, *48*, 4003−4009.
(27) Kang, S. Z.; Yang, Y. K.; Bu, W. B.; Mu, I. *J. Solid State Chem.* **2009**, *182*, 2972−2976.
(28) Tsuji, I.; Kato, H.; Kudo, A. *Chem. Mater.* **2006**, *18*, 1969−1975.
(29) Shen, F.; Que, W.; Liao, Y.; Yin, X. *Ind. Eng. Chem. Res.* **2011**, *50*, 9131−9137.
(30) Zhang, J.; Que, W. X.; Jia, Q. Y.; Zhong, P.; Liao, Y. L.; Ye, X. D.; Ding, Y. C. *J. Alloys Compd.* **2011**, *509*, 7421−7426.
(31) Panthani, M. G.; Akhavan, V.; Goodfellow, B.; Schmidtke, J. P.; Dunn, L.; Dodabalapur, A.; Barbara, P. F.; Korgel, B. A. *J. Am. Chem. Soc.* **2008**, *130*, 16770−16777.
(32) Ingle, J. D. J.; Crouch, S. R. *Spectrochemical Analysis*; Prentice Hall: Upper Saddle River, NJ, 1988.
(33) Fujishima, A.; Zhang, X.; Tryk, D. A. *Surf. Sci. Rep.* **2008**, *63*, 515−582.
(34) Abdullah, A. Z.; Ling, P. Y. *J. Hazard. Mater.* **2010**, *173*, 159−167.
(35) Knox, R. S. *Theory of Excitons, Solid State Physics Supplement 5*; Academic Press: New York, 1963.
(36) Rincon, C.; Marquez, R. *J. Phys. Chem. Solids* **1999**, *60*, 1865−1873.
(37) Czekelius, C.; Hilgendorff, M.; Spanhel, L.; Bedja, I.; Lerch, M.; Muller, G.; Bloeck, U.; Su, D. S.; Giersig, M. *Adv. Mater.* **1999**, *11*, 643−646.
(38) Castro, S. L.; Bailey, S. G.; Raffaelle, R. P.; Banger, K. K.; Hepp, A. F. *Chem. Mater.* **2003**, *15*, 3142−3147.
(39) Jiang, J.; Zhang, X.; Sun, P. B.; Zhang, L. Z. *J. Phys. Chem. C* **2011**, *115*, 20555−20564.